Physics Letters B 673 (2009) 119–126

Contents lists available at ScienceDirect

Physics Letters B

www.elsevier.com/locate/physletb

Inclusive photoproduction of ρ^0, K^{*0} and ϕ mesons at HERA

H1 Collaboration

F.D. Aaron [e,aw], C. Alexa [e], V. Andreev [y], B. Antunovic [k], S. Aplin [k], A. Asmone [ag], A. Astvatsatourov [d], S. Backovic [ad], A. Baghdasaryan [al], E. Barrelet [ac], W. Bartel [k], K. Begzsuren [ai], O. Behnke [n], A. Belousov [y], N. Berger [an], J.C. Bizot [aa], V. Boudry [ab], I. Bozovic-Jelisavcic [b], J. Bracinik [c], G. Brandt [k], M. Brinkmann [k], V. Brisson [aa], D. Bruncko [p], A. Bunyatyan [m,al], G. Buschhorn [z], L. Bystritskaya [x], A.J. Campbell [k], K.B. Cantun Avila [v], F. Cassol-Brunner [u], K. Cerny [af], V. Cerny [p,au], V. Chekelian [z], A. Cholewa [k], J.G. Contreras [v], J.A. Coughlan [f], G. Cozzika [j], J. Cvach [ae], J.B. Dainton [r], K. Daum [ak,aq], M. Deák [k], Y. de Boer [k], B. Delcourt [aa], M. Del Degan [an], J. Delvax [d], A. De Roeck [k,as], E.A. De Wolf [d], C. Diaconu [u], V. Dodonov [m], A. Dossanov [z], A. Dubak [ad,at], G. Eckerlin [k], V. Efremenko [x], S. Egli [aj], A. Eliseev [y], E. Elsen [k], A. Falkiewicz [g], P.J.W. Faulkner [c], L. Favart [d], A. Fedotov [x], R. Felst [k], J. Feltesse [j,av], J. Ferencei [p], D.-J. Fischer [k], M. Fleischer [k], A. Fomenko [y], E. Gabathuler [r], J. Gayler [k], S. Ghazaryan [al], A. Glazov [k], I. Glushkov [am], L. Goerlich [g], N. Gogitidze [y], M. Gouzevitch [ab], C. Grab [an], T. Greenshaw [r], B.R. Grell [k], G. Grindhammer [z], S. Habib [l,1], D. Haidt [k], M. Hansson [t], C. Helebrant [k], R.C.W. Henderson [q], E. Hennekemper [o], H. Henschel [am], M. Herbst [o], G. Herrera [w], M. Hildebrandt [aj], K.H. Hiller [am], D. Hoffmann [u], R. Horisberger [aj], T. Hreus [d,ar], M. Jacquet [aa], M.E. Janssen [k], X. Janssen [d], V. Jemanov [l], L. Jönsson [t], A.W. Jung [o], H. Jung [k], M. Kapichine [i], J. Katzy [k], I.R. Kenyon [c], C. Kiesling [z], M. Klein [r], C. Kleinwort [k], T. Kluge [r], A. Knutsson [k], R. Kogler [z], V. Korbel [k], P. Kostka [am], M. Kraemer [k], K. Krastev [k], J. Kretzschmar [r], A. Kropivnitskaya [x], K. Krüger [o], K. Kutak [k], M.P.J. Landon [s], W. Lange [am], G. Laštovička-Medin [ad], P. Laycock [r], A. Lebedev [y], G. Leibenguth [an], V. Lendermann [o], S. Levonian [k], G. Li [aa], K. Lipka [l], A. Liptaj [z], B. List [l], J. List [k], N. Loktionova [y], R. Lopez-Fernandez [w], V. Lubimov [x], L. Lytkin [m], A. Makankine [i], E. Malinovski [y], P. Marage [d], Ll. Marti [k], H.-U. Martyn [a], S.J. Maxfield [r], A. Mehta [r], K. Meier [o], A.B. Meyer [k], H. Meyer [k], H. Meyer [ak], J. Meyer [k], V. Michels [k], S. Mikocki [g], I. Milcewicz-Mika [g], F. Moreau [ab], A. Morozov [i], J.V. Morris [f], M.U. Mozer [d], M. Mudrinic [b], K. Müller [ao], P. Murín [p,ar], B. Naroska [l,2], Th. Naumann [am], P.R. Newman [c], C. Niebuhr [k], A. Nikiforov [k], G. Nowak [g], K. Nowak [ao], M. Nozicka [k], B. Olivier [z], J.E. Olsson [k], S. Osman [t], D. Ozerov [x], V. Palichik [i], I. Panagoulias [k,ap,3], M. Pandurovic [b], Th. Papadopoulou [k,ap,3], C. Pascaud [aa], G.D. Patel [r], O. Pejchal [af], E. Perez [j,as], A. Petrukhin [x], I. Picuric [ad], S. Piec [am], D. Pitzl [k], R. Plačakytė [k], R. Polifka [af], B. Povh [m], T. Preda [e], V. Radescu [k], A.J. Rahmat [r], N. Raicevic [ad], A. Raspiareza [z], T. Ravdandorj [ai], P. Reimer [ae], E. Rizvi [s], P. Robmann [ao], B. Roland [d], R. Roosen [d], A. Rostovtsev [x], M. Rotaru [e], J.E. Ruiz Tabasco [v], Z. Rurikova [k], S. Rusakov [y], D. Šálek [af], D.P.C. Sankey [f], M. Sauter [an], E. Sauvan [u], S. Schmitt [k], C. Schmitz [ao], L. Schoeffel [j], A. Schöning [k,ao,*], H.-C. Schultz-Coulon [o], F. Sefkow [k], R.N. Shaw-West [c], I. Sheviakov [y], L.N. Shtarkov [y], S. Shushkevich [z], T. Sloan [q], I. Smiljanic [b], Y. Soloviev [y], P. Sopicki [g], D. South [h], V. Spaskov [i], A. Specka [ab], Z. Staykova [k], M. Steder [k], B. Stella [ag], G. Stoicea [e], U. Straumann [ao], D. Sunar [d], T. Sykora [d], V. Tchoulakov [i], G. Thompson [s], P.D. Thompson [c], T. Toll [k], F. Tomasz [p], T.H. Tran [aa], D. Traynor [s], T.N. Trinh [u], P. Truöl [ao], I. Tsakov [ah], B. Tseepeldorj [ai,ax], J. Turnau [g], K. Urban [o], A. Valkárová [af], C. Vallée [u], P. Van Mechelen [d], A. Vargas Trevino [k], Y. Vazdik [y], S. Vinokurova [k], V. Volchinski [al], M. von den Driesch [k], D. Wegener [h], Ch. Wissing [k], E. Wünsch [k], J. Žáček [af], J. Zálešák [ae], Z. Zhang [aa], A. Zhokin [x], T. Zimmermann [an], H. Zohrabyan [al], F. Zomer [aa]

[a] *I. Physikalisches Institut der RWTH, Aachen, Germany* [4]
[b] *Vinca Institute of Nuclear Sciences, Belgrade, Serbia*
[c] *School of Physics and Astronomy, University of Birmingham, Birmingham, UK* [5]
[d] *Inter-University Institute for High Energies ULB-VUB, Brussels, Universiteit Antwerpen, Antwerpen, Belgium* [6]
[e] *National Institute for Physics and Nuclear Engineering (NIPNE), Bucharest, Romania*
[f] *Rutherford Appleton Laboratory, Chilton, Didcot, UK* [5]
[g] *Institute for Nuclear Physics, Cracow, Poland* [7]
[h] *Institut für Physik, TU Dortmund, Dortmund, Germany* [4]
[i] *Joint Institute for Nuclear Research, Dubna, Russia*
[j] *CEA, DSM/Irfu, CE-Saclay, Gif-sur-Yvette, France*

0370-2693
doi:10.1016/j.physletb.2009.02.016

[k] DESY, Hamburg, Germany
[l] Institut für Experimentalphysik, Universität Hamburg, Hamburg, Germany [4]
[m] Max-Planck-Institut für Kernphysik, Heidelberg, Germany
[n] Physikalisches Institut, Universität Heidelberg, Heidelberg, Germany [4]
[o] Kirchhoff-Institut für Physik, Universität Heidelberg, Heidelberg, Germany [4]
[p] Institute of Experimental Physics, Slovak Academy of Sciences, Košice, Slovak Republic [9]
[q] Department of Physics, University of Lancaster, Lancaster, UK [5]
[r] Department of Physics, University of Liverpool, Liverpool, UK [5]
[s] Queen Mary and Westfield College, London, UK [5]
[t] Physics Department, University of Lund, Lund, Sweden [10]
[u] CPPM, CNRS/IN2P3 - Univ. Mediterranee, Marseille, France
[v] Departamento de Fisica Aplicada, CINVESTAV, Mérida, Yucatán, Mexico [13]
[w] Departamento de Fisica, CINVESTAV, Mexico [13]
[x] Institute for Theoretical and Experimental Physics, Moscow, Russia [14]
[y] Lebedev Physical Institute, Moscow, Russia [8]
[z] Max-Planck-Institut für Physik, München, Germany
[aa] LAL, Univ Paris-Sud, CNRS/IN2P3, Orsay, France
[ab] LLR, Ecole Polytechnique, IN2P3-CNRS, Palaiseau, France
[ac] LPNHE, Universités Paris VI and VII, IN2P3-CNRS, Paris, France
[ad] Faculty of Science, University of Montenegro, Podgorica, Montenegro [8]
[ae] Institute of Physics, Academy of Sciences of the Czech Republic, Praha, Czech Republic [11]
[af] Faculty of Mathematics and Physics, Charles University, Praha, Czech Republic [11]
[ag] Dipartimento di Fisica, Università di Roma Tre and INFN Roma 3, Roma, Italy
[ah] Institute for Nuclear Research and Nuclear Energy, Sofia, Bulgaria [8]
[ai] Institute of Physics and Technology of the Mongolian Academy of Sciences, Ulaanbaatar, Mongolia
[aj] Paul Scherrer Institut, Villigen, Switzerland
[ak] Fachbereich C, Universität Wuppertal, Wuppertal, Germany
[al] Yerevan Physics Institute, Yerevan, Armenia
[am] DESY, Zeuthen, Germany
[an] Institut für Teilchenphysik, ETH, Zürich, Switzerland [12]
[ao] Physik-Institut der Universität Zürich, Zürich, Switzerland [12]
[ap] Also at Physics Department, National Technical University, Zografou Campus, GR-15773 Athens, Greece
[aq] Also at Rechenzentrum, Universität Wuppertal, Wuppertal, Germany
[ar] Also at University of P.J. Šafárik, Košice, Slovak Republic
[as] Also at CERN, Geneva, Switzerland
[at] Also at Max-Planck-Institut für Physik, München, Germany
[au] Also at Comenius University, Bratislava, Slovak Republic
[av] Also at DESY and University Hamburg, Helmholtz Humboldt Research Award, Germany
[aw] Also at Faculty of Physics, University of Bucharest, Bucharest, Romania
[ax] Also at Ulaanbaatar University, Ulaanbaatar, Mongolia

ARTICLE INFO

Article history:
Received 5 January 2009
Received in revised form 6 February 2009
Accepted 9 February 2009
Available online 12 February 2009
Editor: W.-D. Schlatter

ABSTRACT

Inclusive non-diffractive photoproduction of $\rho(770)^0$, $K^*(892)^0$ and $\phi(1020)$ mesons is investigated with the H1 detector in ep collisions at HERA. The corresponding average γp centre-of-mass energy is 210 GeV. The mesons are measured in the transverse momentum range $0.5 < p_T < 7$ GeV and the rapidity range $|y_{\rm lab}| < 1$. Differential cross sections are presented as a function of transverse momentum and rapidity, and are compared to the predictions of hadroproduction models.

1. Introduction

High energy particle collisions, which give rise to large multiplicities of produced hadrons, provide an opportunity to study the hadronisation process, whereby the quarks and gluons produced in the initial interaction become colourless hadrons. Since most of these hadrons are produced at low values of transverse momentum, perturbative quantum chromodynamics (pQCD) is not applicable to this process, which is described instead using phenomenological models, the most successful of which are the string [1] and the cluster [2] fragmentation models. These can provide a reasonable description of the hadronisation process provided the many free parameters they contain are tuned to the data.

The production of long-lived hadrons and resonances at high energies has been studied in detail in electron–positron (e^+e^-) collisions at LEP using Z^0 decays [3]. Measurements in high energy hadronic interactions have so far been restricted to long-lived hadrons and hadrons containing heavy quarks. Recently, the

* Corresponding author at: DESY, Hamburg, Germany.
E-mail address: schoning@mail.desy.de (A. Schöning).

[1] Supported by a scholarship of the World Laboratory Björn Wiik Research Project.
[2] Deceased.
[3] This project is co-funded by the European Social Fund (75%) and National Resources (25%) - (EPEAEK II) - PYTHAGORAS II.
[4] Supported by the Bundesministerium für Bildung und Forschung, FRG, under contract numbers 05 H1 1GUA/1, 05 H1 1PAA/1, 05 H1 1PAB/9, 05 H1 1PEA/6, 05 H1 1VHA/7 and 05 H1 1VHB/5.
[5] Supported by the UK Science and Technology Facilities Council, and formerly by the UK Particle Physics and Astronomy Research Council.
[6] Supported by FNRS-FWO-Vlaanderen, IISN-IIKW and IWT and by Interuniversity Attraction Poles Programme, Belgian Science Policy.
[7] Partially Supported by Polish Ministry of Science and Higher Education, grant PBS/DESY/70/2006.
[8] Supported by the Deutsche Forschungsgemeinschaft.
[9] Supported by VEGA SR grant No. 2/7062/27.
[10] Supported by the Swedish Natural Science Research Council.
[11] Supported by the Ministry of Education of the Czech Republic under the projects LC527, INGO-1P05LA259 and MSM0021620859.
[12] Supported by the Swiss National Science Foundation.
[13] Supported by CONACYT, México, grant 48778-F.
[14] Russian Foundation for Basic Research (RFBR), grant no 1329.2008.2.

production of the hadronic resonances $\rho(770)^0$, $K^*(892)^0$ and $\phi(1020)$ has been measured in heavy-ion and proton–proton (pp) collisions at RHIC [4]. The electron–proton (ep) collider HERA allows the study of particle production in quasi-real photon–proton (γp) collisions. The comparison of RHIC and HERA results is of particular interest, since the nuclear density at HERA is much lower than that at RHIC while the γp and nucleon–nucleon collision energies are similar.

In this Letter, measurements of the inclusive non-diffractive photoproduction of the resonances $\rho(770)^0$, $K^*(892)^0$ and $\phi(1020)$ at HERA are presented for the first time. The measurements are based on the data recorded with the H1 detector during the year 2000, when positrons of energy 27.6 GeV collided with 920 GeV protons at an ep centre-of-mass energy of 319 GeV, providing on average a γp centre-of-mass energy of $\langle W \rangle = 210$ GeV. The data correspond to an integrated luminosity of $\mathcal{L} = 36.5$ pb^{-1}.

2. Phenomenology and Monte Carlo simulation

The H1 coordinate system has as its origin the position of the nominal interaction vertex. The outgoing proton beam direction defines the positive z-axis and is also referred to as the "forward" direction. The polar angle θ is defined with respect to this direction. The pseudorapidity is given by $\eta_{\rm lab} = -\ln(\tan(\theta/2))$. The laboratory frame rapidity $y_{\rm lab}$ of a particle with energy E and longitudinal momentum p_z is given by $y_{\rm lab} = 0.5 \ln[(E+p_z)/(E-p_z)]$.

The invariant differential cross section for meson production can be expressed as a function of the meson's transverse momentum p_T and its rapidity $y_{\rm lab}$, assuming azimuthal symmetry. Hadrons produced in hadronic collisions are approximately uniformly distributed in the central rapidity range, while their transverse momentum spectra fall steeply with increasing p_T. It is convenient to parametrise the invariant differential cross section of the produced hadrons with a power law distribution,

$$\frac{1}{\pi}\frac{d^2\sigma^{\gamma p}}{dp_T^2\, dy_{\rm lab}} = \frac{A}{(E_{T_0} + E_T^{\rm kin})^n}, \tag{1}$$

where $E_T^{\rm kin} = \sqrt{m_0^2 + p_T^2} - m_0$ is the transverse kinetic energy, m_0 is the nominal resonance mass, A is a normalisation factor independent of p_T and E_{T_0} a free parameter. When $E_T^{\rm kin} \lesssim E_{T_0}$, the power law function (1) behaves like a Boltzmann distribution $\exp(-E_T^{\rm kin}/T)$, with $T = E_{T_0}/n$. This exponential behaviour of hadronic spectra follows from a thermodynamic model of hadroproduction [5]. In this framework, the parameter T plays the role of the temperature at which hadronisation takes place. At high $E_T^{\rm kin}$, the power law originates from a convolution of the parton densities of the colliding particles with the cross sections of parton–parton interactions. The normalisation coefficient A is related to the single differential cross section $d\sigma/dy_{\rm lab}$ obtained after the integrating Eq. (1) over p_T^2:

$$A = \frac{d\sigma}{dy_{\rm lab}} \frac{(n-1)(n-2)(E_{T_0})^{n-1}}{2\pi(E_{T_0} + (n-2)m_0)}. \tag{2}$$

Monte Carlo calculations are used both to correct the data and in comparisons with the measurements. Direct and resolved photoproduction events are simulated using the PYTHIA [6] and the PHOJET [7] Monte Carlo generators. In both cases, the hadronisation is based on the string fragmentation model [8]. For data corrections, the parameter settings obtained by the ALEPH Collaboration [9] are used for the fragmentation of partons. The effects of Bose–Einstein correlations (BEC) on the invariant mass spectra of like-sign and unlike-sign pion pairs are included using a Gaussian parametrisation of the correlation function [9]. The photoproduction events generated using PYTHIA and PHOJET are passed through the simulation of the H1 detector based on GEANT [10] and through the same reconstruction and analysis chain as used for the data.

3. Experimental conditions

3.1. H1 detector

The H1 detector is described in detail elsewhere [11]. A brief account of the components that are most relevant to the present analysis is given here.

The ep interaction region is surrounded by two large concentric drift chambers (CJCs), operated inside a 1.16 T solenoidal magnetic field. Charged particles are measured in the pseudorapidity range $-1.5 < \eta_{\rm lab} < 1.5$ with a transverse momentum resolution of $\sigma_{p_T}/p_T \approx 0.005 \cdot p_T/\text{GeV} \oplus 0.015$ [12]. The specific energy loss dE/dx of the charged particles is measured in this detector with a relative resolution of 7.5% for a minimum ionising track [13].

A finely segmented electromagnetic and hadronic liquid argon calorimeter (LAr) covers the range $-1.5 < \eta_{\rm lab} < 3.4$. The energy resolution of this calorimeter is $\sigma(E)/E = 0.11/\sqrt{E/\text{GeV}}$ for electromagnetic showers and $\sigma(E)/E = 0.50/\sqrt{E/\text{GeV}}$ for hadrons as measured in test beams [14].

Photoproduction events are selected with a crystal Čerenkov calorimeter (positron tagger) located close to the beam pipe at $z = -33.4$ m, which measures the energy deposited by positrons scattered at angles of less than 5 mrad. Another Čerenkov calorimeter, located at $z = -103$ m (photon tagger), is used to determine the luminosity by measuring the rate of photons emitted in the Bethe–Heitler process $ep \to ep\gamma$.

3.2. Event selection

Photoproduction events are selected by a trigger which requires a scattered positron to be measured in the positron tagger, an event vertex determined from charged tracks and three or more charged tracks reconstructed in the CJCs, each with transverse momentum $p_T > 0.4$ GeV. The photon virtuality Q^2 is smaller than 0.01 GeV^2, due to the positron tagger acceptance. The photon energy is determined from the difference between the positron beam energy and the energy measured in the positron tagger.

In order to reduce the non-ep background and to ensure good reconstruction of the event kinematics, the following criteria are applied:

- Events are selected if the reconstructed γp centre-of-mass energy lies within the interval $174 < W < 256$ GeV for which good positron detection efficiency is established. This corresponds to an average γp centre-of-mass energy of $\langle W \rangle = 210$ GeV.
- Events are rejected if a photon with energy $E_\gamma > 2$ GeV is detected in the photon tagger. This suppresses the background arising from random coincidences of Bethe–Heitler events in the positron tagger with beam-gas interactions in the main H1 detector.
- Events are selected if the z coordinate of the event vertex, reconstructed using the CJCs, lies within 35 cm of the mean position for ep interactions.

Background from elastic and diffractive events is suppressed by the above trigger requirements. To further reduce the contribution of diffractive processes, the presence of an energy deposit of at least 500 MeV is required in the forward region of the LAr, defined by $2.03 < \eta_{\rm lab} < 3.26$. Monte Carlo studies show that, with this requirement, less than 1% of the final event sample consists of

diffractive events with $X_{\mathbb{P}} < 0.05$, where $X_{\mathbb{P}} = M_X^2/W^2$ and M_X is the invariant mass of the diffractive system.

In total, about 1.8×10^6 events satisfy the above selection criteria.

3.3. Selection of $\rho(770)^0$, $K^*(892)^0$ and $\phi(1020)$ mesons

The mesons are identified using the $\rho(770)^0 \to \pi^+\pi^-$, $K^*(892)^0 \to K^+\pi^-$ or $\bar{K}^*(892)^0 \to K^-\pi^+$ and $\phi(1020) \to K^+K^-$ decays.[15] Charged tracks reconstructed in the CJCs with $p_T > 0.15$ GeV and pseudorapidity $|\eta_{\rm lab}| < 1.5$ are considered as charged pion or kaon candidates. Since most of the charged particles in ep collisions are pions, no attempt to identify pions is made, while identification criteria for charged kaons are applied for the extraction of the K^{*0} and ϕ signals. This is done by measuring the momentum-dependent specific energy loss dE/dx in the CJCs. This method gives a significant improvement in the signal-to-background ratio for low p_T mesons, $p_T < 1.5$ GeV, where the dE/dx resolution allows good particle identification. For high p_T mesons, $p_T > 1.5$ GeV, the dE/dx method is inefficient and therefore particle identification criteria are not applied. Such tracks are considered as both pion and kaon candidates and their four-momenta are determined from the track measurements using the corresponding mass hypothesis [15]. Vector meson candidates are reconstructed from these four-momenta. The kinematic range for the reconstructed neutral mesons is restricted to $|y_{\rm lab}| < 1$ and $p_T > 0.5$ GeV.

To extract the ρ^0, K^{*0} and ϕ signals, the distributions of respective invariant masses of their decay products, $m_{\pi^+\pi^-}$, $m_{K^\pm\pi^\mp}$ and $m_{K^+K^-}$, are fitted using a function composed of three parts:

$$F(m) = B(m) + \sum R(m) + \sum S(m). \tag{3}$$

The terms correspond to contributions from the combinatorial background, $B(m)$, from reflections which result from decays other than the signal under consideration, $R(m)$, and from the relevant signal, $S(m)$, respectively.

The combinatorial background function is taken to be:

$$B(m) = \left(a_0 + a_1 m + a_2 m^2 + a_3 m^3\right) \cdot B^0(m),$$

where a_0, a_1, a_2 and a_3 are free parameters, and $B^0(m)$ is the invariant mass distribution of the like-sign charged particle combinations: $\pi^\pm\pi^\pm$ for the ρ^0 and $K^\pm\pi^\pm$ for the K^{*0}. The shape of the combinatorial background for ϕ is described by the following function:

$$B(m) = b_1\left(m^2 - 4m_K^2\right)^{b_2} e^{-b_3 m},$$

where b_1, b_2 and b_3 are free parameters and m_K is the kaon mass.

The second term, $\sum R(m)$, in (3) represents the sum of the reflections; for example, charged particles from the decay $K^{*0} \to K^\pm\pi^\mp$ with the kaon misidentified as a charged pion will give rise to structure in the $m_{\pi^+\pi^-}$ spectrum and must be taken into account as a separate contribution. In addition, there are two other contributions to the $m_{\pi^+\pi^-}$ spectrum in the mass region of interest. These arise from the decays $\omega(782) \to \pi^+\pi^-$ and $\omega(782) \to \pi^+\pi^-\pi^0$ in which the π^0 is not observed. For the $\omega(782)$ meson, the production rate relative to that of the ρ^0 is varied within the range 1.0 ± 0.2, which is consistent with measurements of the $\omega(782)/\rho^0$ ratio in hadronic collisions [16] and in Z^0 boson decays [17]. The $\omega(782)$ branching ratios are taken from [15]. The five major reflections in the $m_{K^\pm\pi^\mp}$ spectrum are due to: the decay $\rho^0 \to \pi^+\pi^-$ with the π^+ or π^- misidentified as a charged kaon; the decays $\omega(782) \to \pi^+\pi^-$ and $\omega(782) \to \pi^+\pi^-\pi^0$ with the π^0 not observed and with one of the π^+ or π^- mesons misidentified as a charged kaon; the decay $\phi \to K^+K^-$ with one of the kaons misidentified as a charged pion and a self-reflection from the K^{*0}, where the pion and kaon are interchanged. For the $m_{K^+K^-}$ spectrum, there are no reflections from known resonances in the invariant mass region of interest. Therefore, the shapes of the reflections are taken from Monte Carlo calculations. The contribution of the reflections from the ρ^0, K^{*0} and ϕ mesons is tied to the production rates determined in this analysis and is therefore iteratively calculated.

The function $S(m)$ used to describe the signal in (3) is a convolution of a relativistic Breit–Wigner function $BW(m)$ and a detector resolution function $r(m, m')$. The relativistic Breit–Wigner function

$$BW(m) = A_0 \frac{m_0 m \Gamma(m)}{(m^2 - m_0^2)^2 + m_0^2 \Gamma^2(m)}, \tag{4}$$

is used with

$$\Gamma(m) = \Gamma_0 \left(\frac{q}{q_0}\right)^{2l+1} \frac{m_0}{m},$$

where A_0 is a normalisation factor, Γ_0 is the resonance width, $l = 1$ for vector mesons, m_0 is the resonance mass, q is the momentum of the decay products in the rest frame of the parent meson, and q_0 is their momentum at $m = m_0$. The cross sections cited in this Letter assume that the meson signal is defined as the integral of the relativistic Breit–Wigner function (4) in the region $\pm 2.5\Gamma_0$ around the mass m_0. Monte Carlo studies show that a non-relativistic Breit–Wigner function with width $\Gamma_{\rm res}$ provides a good description of the detector resolution function:

$$r(m, m') = \frac{1}{2\pi} \frac{\Gamma_{\rm res}}{(m - m')^2 + (\Gamma_{\rm res}/2)^2}. \tag{5}$$

For the K^{*0} analysis, the resolution parameter is determined from Monte Carlo with $\Gamma_{\rm res} = 12$ MeV. It is small compared to the width of the K^{*0} meson (50.3 ± 0.6 MeV) [15], leading only to a small change in the shape of the resonance. For the ϕ, $\Gamma_{\rm res}$ is comparable to the width of the ϕ meson ($\Gamma_0 = 4.26 \pm 0.05$ MeV) [15]. As a result, the shape of the ϕ signal is significantly changed, and hence the detector resolution $\Gamma_{\rm res}$ is taken as a free parameter in the fit. It is found to vary from 3.4 MeV to 6.0 MeV, increasing with the p_T of the ϕ meson.

For the ρ^0 meson, the detector resolution is significantly smaller than its width. However, BEC between the ρ^0 decay pions and other pions in the event strongly distort the ρ^0 line shape. The BEC plays an important role in broadening the ρ^0 mass peak and in shifting it towards lower masses. Similar effects are observed in pp and heavy-ion collisions at RHIC [4] and in e^+e^- collisions at LEP using Z^0 decays [17]. It is therefore important to check that the Monte Carlo model used for the extraction of the cross sections describes the di-pion spectra in the data. The data spectra and the Monte Carlo simulations with and without BEC are shown in Fig. 1. The Monte Carlo model with BEC is in a good agreement with the data in the region of the ρ^0 resonance, whereas the model without BEC fails to describe the di-pion mass spectrum.

The results of fitting the function (3) to the $m_{\pi^+\pi^-}$ data in the mass range from 0.45 to 1.7 GeV with the contributions due to the combinatorial background and the reflections are shown in Fig. 2(a), and after combinatorial background subtraction in Fig. 2(b). In this mass range, the signal from the K^0_S, $f_0(980)$ and $f_2(1270)$ mesons is taken into account. The K^0_S signal is fitted using a Gaussian centred on the nominal mass and with fixed width. The relativistic Breit–Wigner function given in Eq. (4) is used for the $f_0(980)$ and $f_2(1270)$ mesons. In the fit, the resonance masses m_0 and the yields are free parameters. The ρ^0 and $f_2(1270)$ widths

[15] In the following, the notation K^{*0} is used to refer to both the K^{*0} and $\bar{K}^{*0}$ mesons unless explicitly stated otherwise.

are fixed to the Particle Data Group [15] values and the $f_0(980)$ width is fixed to 70 MeV. Due to the small signal and the non-trivial background behaviour, which lead to large uncertainties, cross sections for $f_0(980)$ and $f_2(1270)$ meson production are not measured here.

The K^{*0} signal is measured under the assumption that there is no difference between the particle and antiparticle production rates, and the signal obtained from the $m_{K^\pm\pi^\mp}$ spectrum is divided by 2 to determine the K^{*0} rate in the following. The result of fitting the function (3) to the $m_{K^\pm\pi^\mp}$ data in the mass range from 0.7 to 1.2 GeV with the contributions due to the combinatorial background and the reflections is shown in Fig. 2(c). In the fit, the K^{*0} width is fixed to the nominal value while the mass parameter is left free. The result for the K^{*0} mass is compatible with the world average [15].

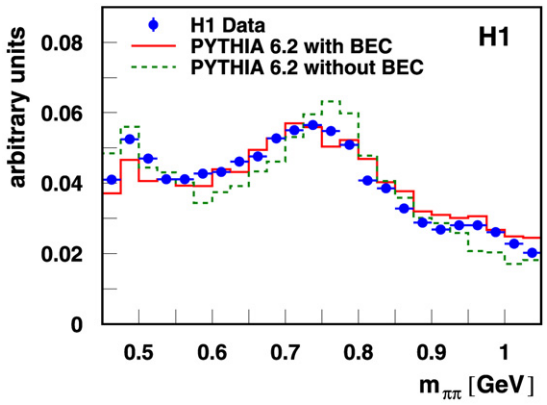

Fig. 1. The unlike-sign di-pion mass spectrum after subtracting the like-sign contribution, normalised to the total number of entries. The solid and dashed curves correspond to the PYTHIA simulation with and without Bose–Einstein correlations (BEC), respectively.

The result of fitting function (3) to the $m_{K^+K^-}$ data in the mass range from 0.99 to 1.06 GeV, together with the background contribution, is shown in Fig. 2(d). In the fit, the ϕ width, Γ_0, is fixed to the nominal value while the mass is left a free parameter and is found to be compatible with the world average [15].

3.4. Cross section determination and systematic errors

The invariant differential cross section for ρ^0, K^{*0} and ϕ meson production is measured in the $y_{\rm lab}$ region from -1 to 1 in seven bins in transverse momentum from 0.5 to 7 GeV. It is calculated according to:

$$\frac{1}{\pi}\frac{d^2\sigma^{\gamma p}}{dp_T^2\,dy_{\rm lab}} = \frac{N}{\pi\cdot\mathcal{L}\cdot BR\cdot\Phi_\gamma\cdot\epsilon\cdot\Delta p_T^2\cdot\Delta y_{\rm lab}},$$

where N is the number of mesons from the fit in each bin. The corresponding bin widths are $\Delta y_{\rm lab} = 2$ and $\Delta p_T^2 = 2p_T^{\rm bin}\Delta p_T$. Bin centre corrections based on Eq. (1) are applied to define the value of $p_T^{\rm bin}$ at which the differential cross section is measured. $\mathcal{L}$ denotes the integrated luminosity and ϵ the efficiency. The branching fractions BR are taken from [15] and are equal to 1, 0.67 and 0.49 for $\rho^0\to\pi^+\pi^-$, $K^{*0}\to K^\pm\pi^\mp$ and $\phi\to K^+K^-$, respectively. The photon flux $\Phi_\gamma = 0.0127$ is calculated using the Weizsäcker–Williams approximation [18].

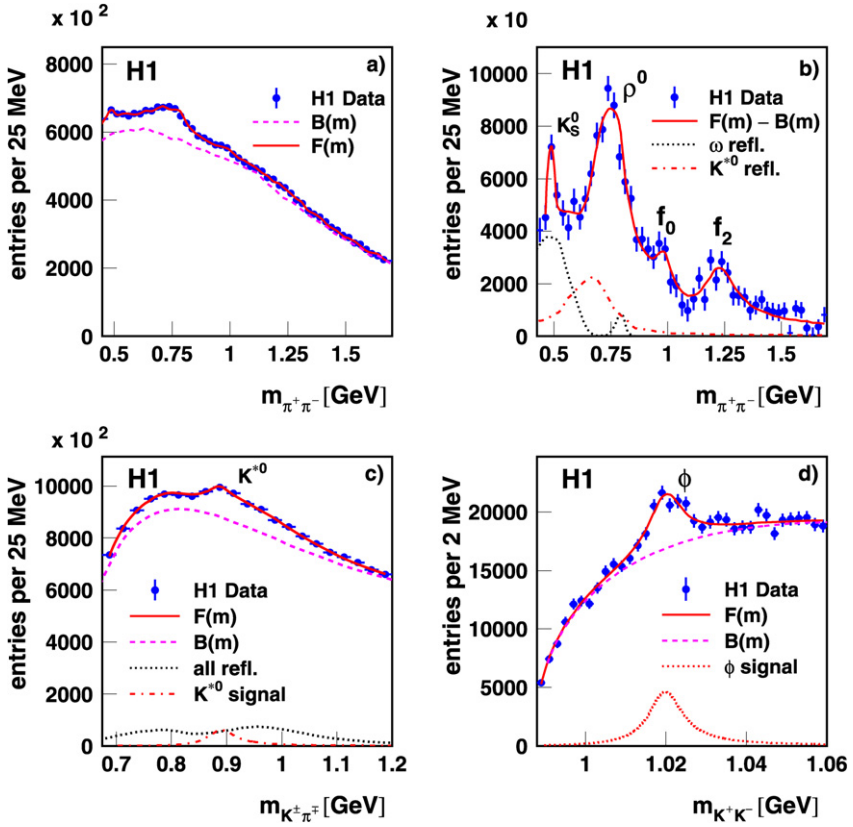

Fig. 2. The invariant mass spectra for $\pi^+\pi^-$ in (a) and (b), for $K^\pm\pi^\mp$ in (c) and for K^+K^- in (d). The full curves show the result of the fit; the dashed curves correspond to the contribution of the combinatorial background $B(m)$. In (b), the data and the fit $F(m)$ are shown after subtraction of the combinatorial background $B(m)$; the dotted and dash-dotted curves show the contributions from ω and K^* reflections, respectively. In (c), the dotted curve corresponds to the contribution of the reflections and the dash-dotted curve corresponds to the contribution of the $K^*(892)$ signal. In (d), the dotted curve corresponds to the contribution of the $\phi(1020)$ signal.

Table 1
Inclusive non-diffractive photoproduction invariant differential cross sections $d^2\sigma/\pi\, dp_T^2\, dy_{\rm lab}$ for $\rho(770)^0$, $K^*(892)^0$ and $\phi(1020)$ mesons in the rapidity range $|y_{\rm lab}| < 1.0$ in bins of p_T. The first error is statistical and the second systematic. For each bin in p_T the range as well as the bin-centred value $p_T^{\rm bin}$ are given.

p_T [GeV]	$p_T^{\rm bin}$	$\frac{1}{\pi}\frac{d^2\sigma}{dp_T^2\, dy_{\rm lab}}$ [nb/(GeV)^2]		
		ρ^0	$(K^{*0}+\bar{K}^{*0})/2$	ϕ
[0.5, 0.75]	0.63	$5610 \pm 870 \pm 590$	$1190 \pm 130 \pm 200$	$383 \pm 54 \pm 60$
[0.75, 1.0]	0.87	$2440 \pm 180 \pm 260$	$621 \pm 68 \pm 80$	$264 \pm 34 \pm 37$
[1.0, 1.5]	1.22	$680 \pm 55 \pm 70$	$176 \pm 18 \pm 21$	$76 \pm 12 \pm 11$
[1.5, 2.0]	1.72	$142 \pm 15 \pm 15$	$48.0 \pm 5.2 \pm 5.1$	$19.1 \pm 3.3 \pm 1.9$
[2.0, 3.0]	2.41	$29.9 \pm 2.3 \pm 3.1$	$8.96 \pm 0.90 \pm 0.98$	$3.48 \pm 0.76 \pm 0.34$
[3.0, 4.0]	3.43	$3.06 \pm 0.42 \pm 0.33$	$1.21 \pm 0.17 \pm 0.14$	$0.46 \pm 0.11 \pm 0.08$
[4.0, 7.0]	5.09	$0.276 \pm 0.037 \pm 0.033$	$0.079 \pm 0.014 \pm 0.009$	$0.0335 \pm 0.0081 \pm 0.0057$

Table 2
Inclusive non-diffractive photoproduction single differential cross sections $d\sigma/dy_{\rm lab}$ for $\rho(770)^0$, $K^*(892)^0$ and $\phi(1020)$ mesons in the transverse momentum range $p_T > 0.5$ GeV in bins of $y_{\rm lab}$. The first error is statistical and the second systematic.

$y_{\rm lab}$	$d\sigma/dy_{\rm lab}$ [μb]		
	ρ^0	$(K^{*0}+\bar{K}^{*0})/2$	ϕ
$[-1.0, -0.5]$	$11.0 \pm 1.0 \pm 1.2$	$3.36 \pm 0.35 \pm 0.72$	$1.44 \pm 0.25 \pm 0.22$
$[-0.5, 0.0]$	$13.1 \pm 1.1 \pm 1.4$	$2.52 \pm 0.27 \pm 0.36$	$1.08 \pm 0.12 \pm 0.16$
[0.0, 0.5]	$10.4 \pm 1.5 \pm 1.1$	$3.07 \pm 0.30 \pm 0.44$	$1.44 \pm 0.13 \pm 0.22$
[0.5, 1.0]	$14.6 \pm 1.3 \pm 1.5$	$4.28 \pm 0.44 \pm 0.79$	$1.61 \pm 0.33 \pm 0.25$

The single differential cross section for ρ^0, K^{*0} and ϕ meson production for $p_T > 0.5$ GeV is measured in four bins in rapidity from -1 to 1 according to:

$$\frac{d\sigma^{\gamma p}}{dy_{\rm lab}} = \frac{N}{\mathcal{L} \cdot BR \cdot \Phi_\gamma \cdot \epsilon \cdot \Delta y_{\rm lab}}.$$

Here, the bin width is $\Delta y_{\rm lab} = 0.5$.

The fit procedure described in the previous section is repeated to determine the number of mesons, N, in each measurement bin, calculated as an integral over the signal function (4) within $\pm 2.5\Gamma_0$ around the meson mass. Similarly, the total visible cross section for ρ^0, K^{*0} and ϕ meson production is measured from the number of mesons fitted in the range $|y_{\rm lab}| < 1$ and $p_T > 0.5$ GeV.

The efficiency is given by $\epsilon = \epsilon_{\rm rec} \cdot \mathcal{A}_{\rm etag} \cdot \mathcal{A}_3 \cdot \epsilon_{\rm trig}$. The reconstruction efficiency for the mesons, $\epsilon_{\rm rec}$, includes the geometric acceptance and the efficiency for track reconstruction. It is calculated using Monte Carlo data and is at least 45% at low p_T and rises to about 90% with increasing p_T. For the acceptance determination, the Monte Carlo generators are reweighted to model the observed p_T-dependences. The average acceptance of the positron tagger, $\mathcal{A}_{\rm etag}$, is about 50%, as determined in [19]. The trigger acceptance, $\mathcal{A}_3$, arises from the requirement that at least three tracks are reconstructed in the CJCs with $p_T > 0.4$ GeV. It is determined from Monte Carlo simulations with PYTHIA and PHOJET and varies from 50% to 95%. The trigger efficiency, $\epsilon_{\rm trig}$, is calculated from the data using monitor triggers. It is about 90%. The efficiencies and acceptances as calculated from the PYTHIA and PHOJET simulation are found to be consistent. Small residual differences, attributed to different track multiplicity predictions, are taken into account in the systematic uncertainties of the measurement.

The statistical error varies from 7 to 15% for the ρ^0, 10 to 18% for the K^{*0} and 13 to 24% for the ϕ meson cross sections. The systematic errors arise from the uncertainties in the track reconstruction efficiency (4%) and the trigger efficiency (up to 6%), the variation of the $f_0(980)$ width by ± 30 MeV in the ρ^0 fit (up to 7%), the uncertainties in the dE/dx kaon identification procedure (6% for the K^{*0} and 12% for the ϕ) and the luminosity calculation (2%), the variation of the background shape (5%) and the variation of the assumptions about the normalisation of the contributions from the reflections (4% for the ρ^0 and up to 15% for the K^{*0}). The total systematic error varies from 10 to 12% for the ρ^0, 11 to 21% for the K^{*0} and 10 to 17% for the ϕ meson cross sections.

4. Results and discussion

The inclusive non-diffractive photoproduction cross sections for $\rho^0(770)$, $K^{*0}(892)$ and $\phi(1020)$ mesons in the kinematic region $Q^2 < 0.01$ GeV^2, $174 < W < 256$ GeV, and for $p_T > 0.5$ GeV and $|y_{\rm lab}| < 1$ are found to be:

$$\sigma_{\rm vis}^{\gamma p}(\gamma p \to \rho^0 X) = 25600 \pm 1800 \pm 2700 \text{ nb},$$
$$\sigma_{\rm vis}^{\gamma p}(\gamma p \to K^{*0} X) = 6260 \pm 350 \pm 860 \text{ nb},$$
$$\sigma_{\rm vis}^{\gamma p}(\gamma p \to \phi X) = 2400 \pm 180 \pm 340 \text{ nb}.$$

The first error is statistical and the second systematic. Note that the K^{*0} cross section is the sum of the particle and antiparticle contributions divided by 2.

The differential cross sections for the photoproduction of ρ^0, K^{*0}, and ϕ mesons are presented in Tables 1 and 2 and in Fig. 3. Within the rapidity range of this measurement, the resonance production rates are constant as a function of rapidity, within errors. The transverse momentum spectra of the ρ^0, K^{*0} and ϕ mesons can be parametrised by function (1), where $d\sigma/dy_{\rm lab}$ in Eq. (2) corresponds to the average value of the cross section over central rapidities, $\langle d\sigma/dy_{\rm lab}\rangle_{|y_{\rm lab}|<1}$. In the fit, the value of the power n is fixed to be 6.7, as derived previously from measurements of charged particle spectra by the H1 Collaboration [20] which gave $n = 6.7 \pm 0.3$. The power law distribution, with this value of n, describes K_S^0 meson, Λ^0 baryon [21] and $D^{*\pm}$ meson production [22] at HERA, as is shown in Fig. 4. A similar shape of the transverse momentum distribution, but with different values of the parameters n and E_{T_0}, was reported for charged particles produced in hadronic collisions [23]. The results of the fits of the data to function (1) are shown in Fig. 3(a). In Table 3, the parameters of the fit and the average transverse kinetic energy $\langle E_T^{\rm kin}\rangle$, the average transverse energy $\langle E_T\rangle = \langle E_T^{\rm kin}\rangle + m_0$ and the average transverse momentum $\langle p_T\rangle = \sqrt{\langle E_T\rangle^2 - m_0^2}$ derived from (1) are presented. The errors include the experimental uncertainty on the value of n. Also given are the $\langle p_T\rangle$ values measured at RHIC in pp and Au–Au collisions [4].

It is interesting to observe that the resonances with different masses, lifetimes and strangeness content are produced with about the same value of the average transverse kinetic energy $\langle E_T^{\rm kin}\rangle$. This observation supports the thermodynamic picture of hadronic interactions [5], in which the primary hadrons are thermalised during the interaction. The values of $\langle p_T\rangle$ for ρ^0, K^{*0} and ϕ mesons are similar in γp and pp collisions with about the same centre-of-mass energy $\sqrt{s} \approx 200$ GeV, while these values are all higher in Au–Au collisions.

The PYTHIA and PHOJET models do not describe the shape of the measured p_T spectra. Moreover, contrary to the data, the

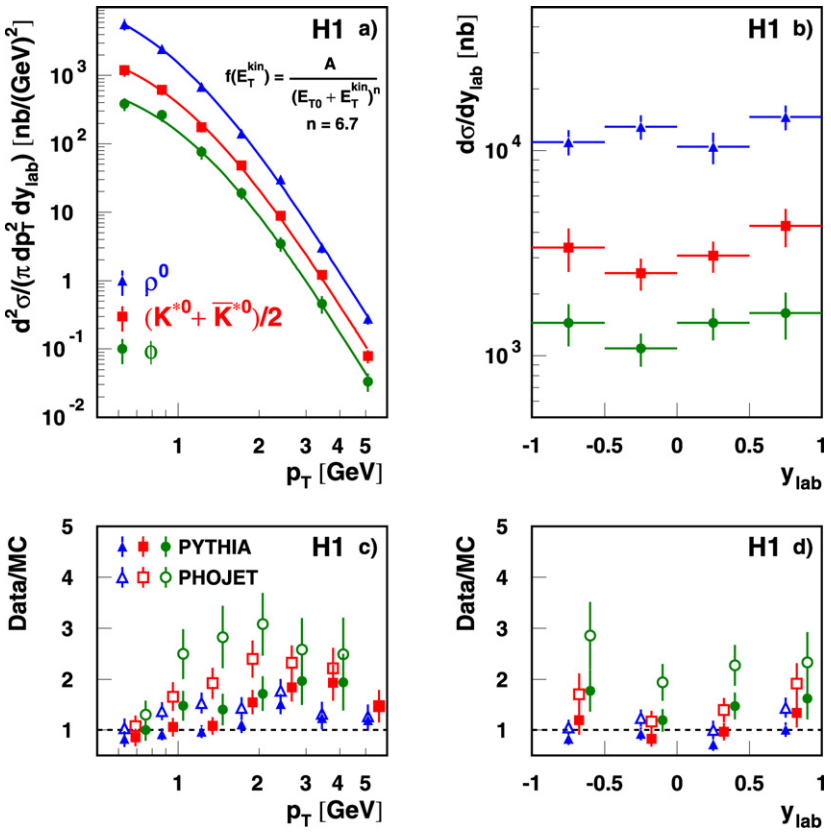

Fig. 3. The inclusive differential non-diffractive cross sections for $\rho^0(770)$, $K^{*0}(892)$ and $\phi(1020)$ mesons measured in (a) as a function of transverse momentum for $|y_{\rm lab}| < 1$ and in (b) as a function of rapidity for $p_T > 0.5$ GeV. The curves on the figure (a) correspond to the power law, Eq. (1), with $n = 6.7$. The ratios of data to Monte Carlo predictions "Data/MC" are shown for the PYTHIA (full points) and PHOJET (empty points) simulations as a function of transverse momentum for $|y_{\rm lab}| < 1$ in (c) and as a function of rapidity for $p_T > 0.5$ GeV in (d). Statistical and systematic errors are added in quadrature.

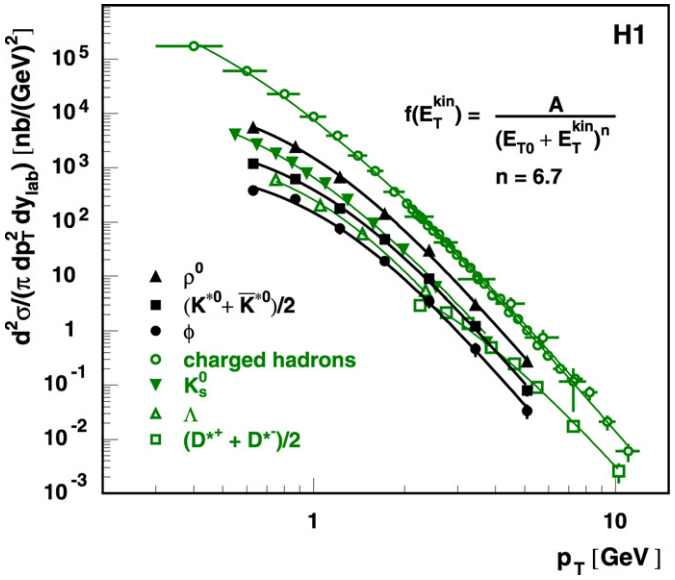

Fig. 4. The inclusive invariant differential cross sections as a function of transverse momentum. The curves show the results of fits to the power law, Eq. (1). Statistical and systematic errors are added in quadrature.

Monte Carlo p_T spectra are not described by the power law function (1). These observations are illustrated in Figs. 3(c) and 3(d).

The measurements in the visible kinematic range of the ρ^0, K^{*0} and ϕ mesons, $p_T > 0.5$ GeV and $|y_{\rm lab}| < 1$, are extrapolated to the full p_T range using the parametrisation (1) to determine the total inclusive non-diffractive photoproduction cross sections.

Table 3
The parameters $\langle d\sigma/dy_{\rm lab}\rangle_{|y_{\rm lab}|<1}$ and $T = E_{T_0}/n$ for ρ^0, K^{*0} and ϕ mesons from a fit of function (1) to the differential cross sections. The average transverse energy $\langle E_T\rangle$, kinetic energy $\langle E_T^{\rm kin}\rangle$ and momentum $\langle p_T\rangle$ are also presented. The errors correspond to the quadratically summed statistical and systematic errors. Also shown are measurements in pp and Au–Au interactions at nucleon–nucleon centre-of-mass energy $\sqrt{s_{NN}} = 200$ GeV [4] at central rapidities.

		ρ^0	$(K^{*0} + \bar{K}^{*0})/2$	ϕ
γp (H1)	$\langle d\sigma/dy_{\rm lab}\rangle_{\lvert y_{\rm lab}\rvert<1}$ [μb]	23.6 ± 2.7	5.22 ± 0.60	1.85 ± 0.23
	T [GeV]	0.151 ± 0.011	0.166 ± 0.012	0.170 ± 0.012
	$\langle E_T\rangle$ [GeV]	1.062 ± 0.018	1.205 ± 0.020	1.333 ± 0.022
	$\langle E_T^{\rm kin}\rangle$ [GeV]	0.287 ± 0.018	0.313 ± 0.020	0.314 ± 0.022
	$\langle p_T\rangle$ [GeV]	0.726 ± 0.027	0.810 ± 0.030	0.860 ± 0.035
pp (STAR)	$\langle p_T\rangle_{pp}$ [GeV]	0.616 ± 0.062	0.81 ± 0.14	0.82 ± 0.03
Au–Au (STAR)	$\langle p_T\rangle_{\rm AuAu}$ [GeV]	0.83 ± 0.10	1.08 ± 0.14	0.97 ± 0.02

Table 4
The ratio $R(\phi/K^{*0})$ of the total cross sections for ϕ and K^{*0} production obtained in γp collisions (H1) at $\langle W\rangle = 210$ GeV. The errors correspond to the quadratically summed statistical and systematic errors. Also shown are measurements in pp and Au–Au interactions at nucleon–nucleon centre-of-mass energy $\sqrt{s_{NN}} = 200$ GeV [4] at central rapidities.

Experiment	Measurement	$R(\phi/K^{*0})$
H1	γp, $\langle W\rangle = 210$ GeV, $\lvert y_{\rm lab}\rvert < 1$	0.354 ± 0.060
STAR	pp, $\sqrt{s} = 200$ GeV, $\lvert y\rvert < 0.5$	0.35 ± 0.05
	Au–Au, $\sqrt{s_{NN}} = 200$ GeV, $\lvert y\rvert < 0.5$	0.63 ± 0.15

The extrapolation factors are of order two. In the rapidity interval $|y_{\rm lab}| < 1$ and integrated over the full p_T range the following cross section ratios are obtained:

$$R\left(K^{*0}/\rho^0\right) = 0.221 \pm 0.036,$$

$R(\phi/\rho^0) = 0.078 \pm 0.013,$

$R(\phi/K^{*0}) = 0.354 \pm 0.060.$

The errors are given by the statistical and systematic errors added in quadrature. PYTHIA and PHOJET, with the strangeness suppression factor $\lambda_s = 0.286$ [9], predict the ratios 0.200, 0.055 and 0.277, respectively, which are similar to the measured values, but are all somewhat lower than these.

In Table 4, $R(\phi/K^{*0})$ is compared to the corresponding ratios measured by STAR in pp and Au–Au collisions [4] at $\sqrt{s_{NN}} = 200$ GeV. Although the rapidity ranges at the H1 and RHIC experiments differ,[16] the resulting ratios for pp and γp interactions are very close. However, the corresponding result in Au–Au collisions is observed to be higher.

5. Conclusions

First measurements of the inclusive non-diffractive photoproduction of $\rho(770)^0$, $K^*(892)^0$ and $\phi(1020)$ mesons at HERA are presented. The differential cross sections for the production of these resonances as a function of transverse momentum are described by a power law distribution while the single differential cross sections as a function of rapidity are observed to be flat in the visible range. Despite their different masses, lifetimes and strangeness content, these resonances are produced with about the same value of the average transverse kinetic energy. This observation supports a thermodynamic picture of hadronic interactions.

The description of the shape of the ρ^0 resonance produced in γp collisions at HERA is improved by taking Bose–Einstein correlations into account. A similar effect is observed in pp and heavy-ion collisions at RHIC and in e^+e^- annihilation at LEP, using Z^0 decays.

The cross section ratios $R(K^{*0}/\rho^0)$, $R(\phi/\rho^0)$ and $R(\phi/K^{*0})$ are determined, and $R(\phi/K^{*0})$ is compared to results obtained in pp and heavy-ion collisions by the STAR experiment at RHIC. The ratio $R(\phi/K^{*0})$ measured in γp interactions is in agreement with the pp results, while this ratio is observed to be smaller than the result obtained in Au–Au collisions.

Acknowledgements

We are grateful to the HERA machine group whose outstanding efforts have made this experiment possible. We thank the engineers and technicians for their work in constructing and maintaining the H1 detector, our funding agencies for financial support, the DESY technical staff for continual assistance and the DESY directorate for support and for the hospitality which they extend to the non-DESY members of the collaboration.

References

[1] B. Andersson, et al., Phys. Rep. 97 (1983) 31.
[2] G.C. Fox, S. Wolfram, Nucl. Phys. B 168 (1980) 285.
[3] A. Boehrer, Phys. Rep. 291 (1997) 107, and references therein.
[4] STAR Collaboration, J. Adams, et al., Phys. Rev. Lett. 92 (2004) 092301;
STAR Collaboration, C. Adler, et al., Phys. Rev. C 71 (2005) 064902;
STAR Collaboration, J. Adams, et al., Phys. Lett. B 612 (2005) 181.
[5] R. Hagedorn, Nuovo Cimento Suppl. 3 (1965) 147.
[6] T. Sjöstrand, L. Lonnblad, S. Mrenna, LU-TP-01-21, PYTHIA 6.2 physics and manual (2001), hep-ph/0108264.
[7] R. Engel, Z. Phys. C 66 (1995) 203;
R. Engel, J. Ranft, Phys. Rev. D 54 (1996) 4244;
PHOJET Monte Carlo generator, version 10.
[8] T. Sjöstrand, Comput. Phys. Commun. 82 (1994) 74.
[9] ALEPH Collaboration, S. Schael, et al., Phys. Lett. B 606 (2005) 265;
ALEPH Collaboration, G. Rudolph, private communication.
[10] R. Brun, et al., GEANT3 User's Guide, CERN-DD/EE/84-1.
[11] H1 Collaboration, I. Abt, et al., Nucl. Instrum. Methods A 386 (1997) 310;
H1 Collaboration, I. Abt, et al., Nucl. Instrum. Methods A 386 (1997) 348.
[12] C. Kleinwort, for the H1 Collaboration, in: Blusk, et al. (Eds.), H1 Alignment Experience, Proceedings of the First LHC Detection Alignment Workshop, CERN, 2006, p. 41, CERN-2007-04.
[13] J. Steinhart, Die Messung des totalen $c\bar{c}$-Photoproduktions-Wirkungsquerschnittes von Λ_c-Baryonen unter Verwendung der verbesserten dE/dx-Teilchenidentifikation am H1-Experiment bei HERA, Ph.D. thesis, Hamburg University, 1999, available at http://www-h1.desy.de/publications/theses_list.html.
[14] H1 Calorimeter Group, B. Andrieu, et al., Nucl. Instrum. Methods A 336 (1993) 499;
H1 Calorimeter Group, B. Andrieu, et al., Nucl. Instrum. Methods A 350 (1994) 57.
[15] W.-M. Yao, et al., J. Phys. G 33 (2006) 1.
[16] Bonn–Hamburg–Munich Collaboration, V. Blobel, et al., Phys. Lett. B 48 (1974) 73.
[17] OPAL Collaboration, P.D. Acton, et al., Z. Phys. C 56 (1992) 521;
ALEPH Collaboration, D. Busculic, et al., Z. Phys. C 69 (1996) 379.
[18] C.F. Weizsäcker, Z. Phys. 88 (1934) 612;
E.J. Williams, Phys. Rev. 45 (1934) 729.
[19] H1 Collaboration, S. Aid, et al., Z. Phys. C 69 (1995) 27.
[20] H1 Collaboration, I. Abt, et al., Phys. Lett. B 328 (1994) 176;
H1 Collaboration, C. Adloff, et al., Eur. Phys. J. C 10 (1999) 363.
[21] H1 Collaboration, C. Adloff, et al., Z. Phys. C 76 (1997) 213.
[22] H1 Collaboration, A. Aktas, et al., Eur. Phys. J. C 50 (2007) 251.
[23] UA1 Collaboration, C. Albajar, et al., Nucl. Phys. B 335 (1990) 261;
CDF Collaboration, F. Abe, et al., Phys. Rev. Lett. 61 (1988) 1819.

[16] The difference in rapidity between the laboratory frame and the γp frame is about two units at H1.